Development of Bioactive Zirconium-Tin Alloy by Combination of Micropores Formation and Apatite Nuclei Deposition

Norihiro Hashimoto[1], Takeshi Yabutsuka[1*], Shigeomi Takai [1]

[1] Department of Fundamental Energy Science, Graduate School of Energy Science, Kyoto University, Yoshida-honmachi, Sakyo-ku, Kyoto 606-8501, Japan
[*]yabutsuka@energy.kyoto-u.ac.jp

Abstract: In previous studies, Zr was obtained apatite-forming ability by various method, however they have taken more than 7 days in SBF to attain apatite-forming ability. In this study, we developed the method to attain apatite-forming ability to Zr alloy within 1 day in SBF by a combination with apatite nuclei that promote apatite formation in SBF. First, Zr-Sn alloy was soaked in concentrated sulfuric acid and pores in micro level were formed on the surface of Zr-Sn alloy. In order to attain apatite forming ability to Zr-Sn alloy, second, apatite nuclei were formed in the micropores. In order to evaluate apatite-forming ability, thus-obtained Zr-Sn alloy with apatite nuclei was soaked in SBF, hydroxyapatite formation was observed on the whole surface of the Zr-Sn alloy plates. From this result, it was clarified that higher apatite-forming ability was attained on the apatite nuclei-treated Zr-Sn alloy with micropores in comparison with that without micropores. When adhesive strength of formed hydroxyapatite film respect to Zr-Sn alloy plates were measured, high adhesive strength of the formed apatite film was attained by forming micropores and subsequently precipitating apatite nuclei in the fabrication process because of an interlocking effect caused by hydroxyapatite formed in the micropores.

1. Introduction

In these days, importance of metals in orthopedic fields has been more and more enlarged because they possessed high mechanical toughness and can be used as bone replacements at highly loaded affected parts such as hip joint and knee joint. Among them, Ti and its alloys have been widely used in both orthopedic and dental fields because of their high bioaffinity. Moreover, Ti and its alloys have sufficient mechanical toughness to apply bone replacement because their corrosion resistance and mechanical strength are proper quality. Recently, in addition, several methodologies for improvement of corrosion resistance and mechanical toughness of Ti alloy has been also proposed [1]. However, Ti and its alloys have a problem in magnetic resonance imaging (MRI) because of metal artifacts derived from their too high magnetism [2]. Thus, Ti and its alloy become magnetized in the strong magnetic field in MRI, they cause metal artifacts which make images obscure and disturb images of organs and tissues around Ti and Ti alloy and they prevent exact diagnose. Hence, it is demanded to develop novel types of metal implants with lower magnetism to prevent such metal artifacts.

Zr and its alloys are characterized by biocompatibility, high corrosion resistance and high mechanical strength similar to Ti and its alloys and also Young's modulus of Zr and its alloys such as Zr-Nb alloy are lower than Ti and its alloys [3,4]. In addition, because magnetic susceptibility of Zr were lower than Ti, Zr is hardly affected by MRI [2]. Furthermore, Zr and its alloys have good in vivo cytocompatibility [2] and they are expected to apply for novel medical materials with bioactivity, superior mechanical properties and the ability to restrain metal artifact. If Zr and its alloys obtain high bioactivity, their clinical applications can be largely extended.

However, it is well known that Zr is not characterized by bioactivity and also does not bond to living bone directly and spontaneously [5]. It is reported that this is because that spontaneous formation of zirconium phosphates on its surface. In order to give the bioactivity to Zr, aqueous NaOH treatment [5], surface coating treatment by ZrO_2/hydroxyapatite composite film [6], hydroxyapatite-based plasma electrolytic oxidation coating method [7], and so on have been proposed by some investigators. However, it is known that most of bioactive ceramics in clinical use show apatite-forming ability in the physiological SBF within 7 days [8] and this is one of the required material properties to bond to living bone, whereas they were not reported to form apatite on the whole surface of Zr related within 7 days immersion in SBF. Therefore, the reduction of immersion time to form apatite on the whole surface of the substrate is important.

In our previous study, we imparted the apatite-forming ability to various bioinert substrates with pores by precipitating fine particles of calcium phosphate which we named apatite nuclei (AN). AN are precipitated by raising pH and temperature of simulated body fluid (SBF) [9-11] properly, and it was found that the precipitated AN actively induce apatite formation in SBF [12,13]. In our previous study, it is succeeded that high bioactivity was attained to stainless steels [14], Co-Cr alloys [15], Ti alloys [16] and Zr [17] by the function of the AN and as the noteworthy result, all substrates were attained apatite-forming ability within 1 day. By precipitating AN on these samples with pores and immersing them in SBF, we succeeded in forming hydroxyapatite on the whole surface of these samples within 1 day.

In this study, we aimed to impart high apatite-forming ability to Zr-Sn alloy by applying above method to precipitate AN and to utilize the function of AN. Firstly, we formed the micropores on the surface of Zr-Sn alloy by soaking in concentrated sulfuric acid. Secondly, we conducted AN

treatment to precipitated AN. Then, we evaluated the apatite-forming ability of thus-treated Zr-Sn alloy by immersing in physiological SBF and investigating hydroxyapatite formation on the surface. Finally, adhesive strength between the hydroxyapatite layer and the Zr-Sn alloy was measured to investigate the usefulness of this method.

2. Materials and Methods

2.1. Preparation of SBF

Reagent-grade NaCl, $NaHCO_3$, KCl, $K_2HPO_4{\cdot}3H_2O$, $MgCl_2{\cdot}6H_2O$, $CaCl_2$ and Na_2SO_4 with the composition as certified in ISO23317 [18] was dissolved in distilled water and buffered at pH 7.40 and 36.5 °C with tris(hydroxymethyl)aminomethane ($(CH_2OH)_3CNH_2$) and 1 M-HCl.

2.2. Preparation of reaction solution (m-SBF)

An aqueous solution was prepared by dissolving 0.228 mg $K_2HPO_4{\cdot}3H_2O$, 0.305 mg $MgCl_2{\cdot}6H_2O$, 0.278 mg $CaCl_2$ and 35 ml 1 M-HCl in distilled water. Then, the volume of the solution was measured up to 1.0 L with distilled water, and the pH was adjusted to 8.20 with $(CH_2OH)_3CNH_2$ at 25 °C. This solution is denoted as 'm-SBF' hereafter and the ion concentrations of SBF and m-SBF is shown in Table 1. In our previous cases, we obtained the result that the amount of AN precipitated by raising both pH and temperature of m-SBF is more than that by raising both pH and temperature of SBF. In this research, therefore, m-SBF was used to precipitate AN.

Table 1. Ion concentration of SBF and m-SBF

	Ion concentration / mM	
	SBF	m-SBF
Na^+	142.0	N/A
K^+	5.0	2.0
Mg^{2+}	1.5	1.5
Ca^{2+}	2.5	2.5
Cl^-	147.8	8.0
HCO_3^-	4.2	N/A
HPO_4^{2-}	1.0	1.0
SO_4^{2-}	0.5	N/A

2.3. Formation of micropores by sulphuric acid treatment

Zr-Sn alloy plates (1.28% Sn, 0.21% Fe, 0.12% Cr, 0.12% O, 0.0094% Si, and Zr as the balance, Nilaco, Japan) with $10 \times 10 \times 0.914$ mm^3 in size were used. First, the surface of the alloy plates was polished by using #400 abrasive paper. Second, the Zr-Sn alloy after polishing were treated by immersing in 95 wt% sulfuric acid (Wako Pure Chemical Industries, Japan) for 72 hours at 60 °C. Finally, the plates were rinsed in distilled water and dried in air. The surface roughness was measured by JIS B 601 using colored 3D laser microscope (VK-9700, KEYENCE, Japan).

2.4. AN treatment

The Zr-Sn alloy plates without and with micropores were soaked in m-SBF, and then Zr-Sn alloy plates with micropores were conducted pressurization treatment by cold isostatic press (CIP) in 100 MPa for 60 min to penetrate m-SBF into micropores. To precipitate the AN, m-SBF in which the Zr-Sn alloy plates without and with micropores were soaked were placed in the 70 °C incubator for 10 hours to heat the m-SBF. After that, the plates were rinsed with distilled water and dried in air.

2.5. Bioactivity evaluation

Bioactivity of the samples were tested by immersing in SBF under the physiological condition (pH 7.40, 36.5 °C) [18]. The surfaces of the plates were analyzed by scanning electron microscopy (SEM; SU6600, Hitachi High-Technologies, Japan) and energy dispersive X-ray analysis (EDX; XFlash® 5010, Bruker, USA), thin film X-ray diffraction (TF-XRD; Rint 2500, Rigaku, Japan), and Fourier transform infrared spectroscopy (FT-IR; FT-720, HORIBA, Japan), and also cross-section of Zr-Sn alloy plates were analyzed by the SEM and EDX.

2.6. Measurement of Ca amount of Zr-Sn alloy surface

The Zr-Sn alloy with AN and with apatite layer formed by immersing in SBF for 1, 4 and 14 days were immersed in 1M HCl and AN or apatite layer formed on the surface were dissolved. After that, Ca concentration in these HCl solution were measured by inductively coupled plasma atomic emission spectroscopy (ICPS-7150, SHIMADZU, Japan) to evaluate amount of Ca on the surface of the substrate.

2.7 Measurement of adhesive strength of apatite layer

Adhesive strength of apatite film formed by soaking in SBF for 14 days respect to Zr-Sn alloy plate was evaluated by modified ASTM C633 method [19,20]. The surfaces of the plates were fixed to stainless steel jigs by Araldite® epoxy glue. Then, tensile load was applied at 1 $mm{\cdot}min^{-1}$ of cross-head speed by universal testing machine (AGS-H Autograph, Shimadzu, Japan). Average values of maximum loads when fractures occurred were obtained.

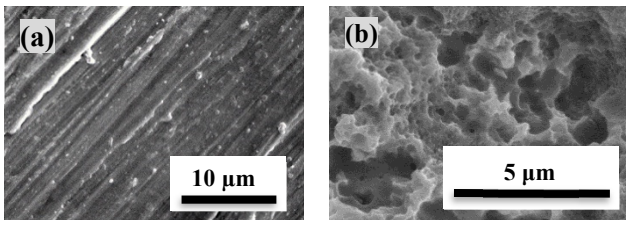

Fig. 1. *SEM images of Zr-Sn alloy plate* ***(a)*** *after polishing and* ***(b)*** *subsequent after sulfuric acid treatment*

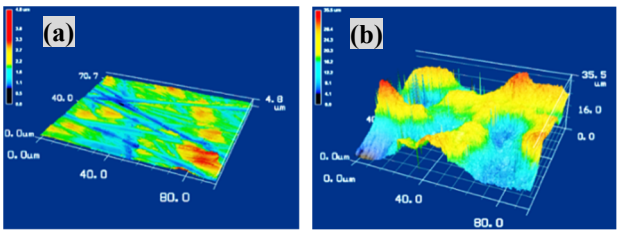

Fig. 2. *3D laser microscope images of the surface of Zr-Sn alloy* ***(a)*** *after polishing and* ***(b)*** *after subsequent sulfuric acid treatment*

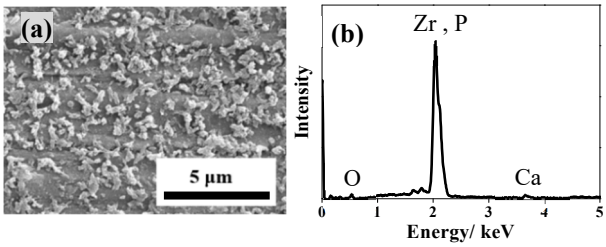

Fig. 3. ***(a)*** *SEM image and* ***(b)*** *EDX profile of the surface of the Zr-Sn alloy without micropores after the AN treatment*

3. Results and discussion

Fig. 1 shows the SEM images of the surface of Zr-Sn alloy after polishing and after subsequent sulfuric acid treatment. Smooth surface was observed on the surface of Zr-Sn alloy plates after polishing. On the other hand, the micropores around 500 nm in size were observed on the whole surface of Zr-Sn alloy plates after sulfuric acid treatment. From these images, it is indicated that the micropores around 500 nm in size were formed by sulfuric acid treatment. Ban et al. obtained micropores with similar shape on the pure Ti by sulfuric acid treatment [24]. Our results show that sulfuric acid treatment was effective also to Zr-Sn alloy probably because Ti and Zr are homologous elements and their substantial property is relatively similar.

Fig. 2 shows the 3D images of the surface of the Zr-Sn alloy both without and with sulfuric acid treatment. After the sulfuric acid treatment, highly roughened surface was observed also by the 3D observation. The surface roughness of both substrates is shown in Table 2. After the sulfuric acid treatment, both Ra and Rz drastically increased. This result corresponded to the results of the SEM observation shown in Fig. 1.

Table 2 Change in surface roughness by sulfuric acid treatment (measured by JIS B0601:2001)

	Without sulfuric acid treatment	With sulfuric acid treatment
Ra (µm)	0.341 ± 0.156	4.411 ± 1.108
Rz (µm)	4.646 ± 0.795	33.171 ± 4.302

Fig. 3 and Fig. 4 show the SEM images and the EDX profiles of the surface of the Zr-Sn alloy without and with micropores after the AN treatment, respectively. From the SEM observation, the particles around 500 nm in size were observed on the whole surface of the Zr-Sn alloy. The EDX profiles in both conditions show the peak of Ca which is the main constituent element of the AN. The main peak of the P was almost overlapped with that of Zr. Except the roughened surface generated by the sulfuric acid treatment, morphologies and elemental characteristics were almost similar among two conditions.

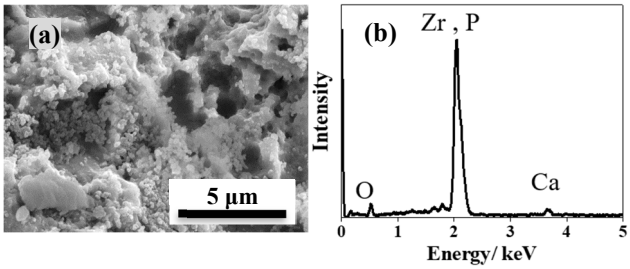

Fig. 4. ***(a)*** *SEM image and* ***(b)*** *EDX profile of the surface of the Zr-Sn alloy with micropores after the AN treatment*

Fig. 5 shows the FT-IR profiles and the TF-XRD profiles of the surfaces of the Zr-Sn alloy after polishing, Zr-Sn alloy without micropores after the AN treatment, the Zr-Sn alloys without micropores and with AN after immersing in SBF for 1 day and 4 days. The FT-IR spectra showed the P-O stretching around 560 cm^{-1} and around 1000 cm^{-1} after the AN treatment. These results show that the particles formed on the surface of Zr-Sn alloy after AN treatment were calcium phosphate. In the TF-XRD profiles, in addition, there were not diffraction peaks of calcium phosphate crystals such as hydroxyapatite. It is indicated that the AN formed on the surface of the Zr-Sn alloy without sulfuric acid treatment were calcium phosphate with extremely low crystallinity such as amorphous calcium phosphate (ACP).

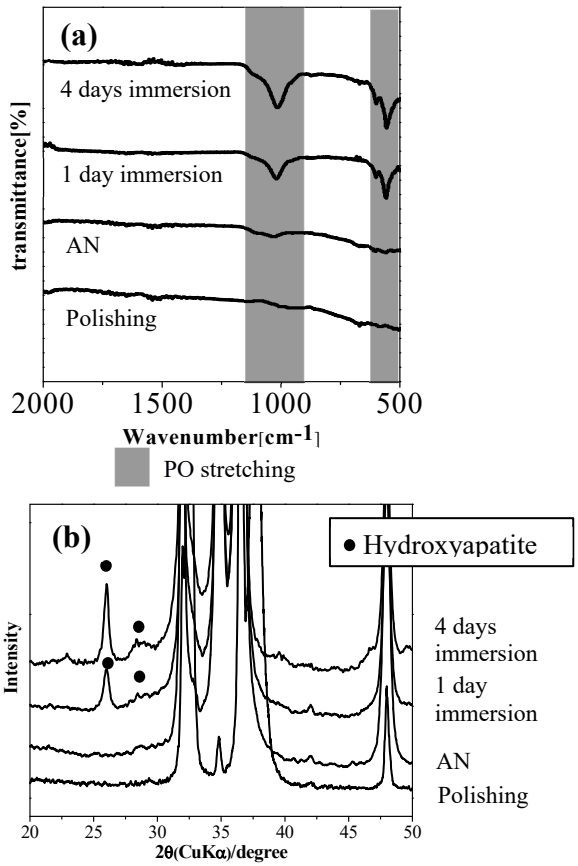

Fig. 5. (a) *FT-IR and* ***(b)*** *TF-XRD profiles of the surface of the untreated Zr-Sn alloy, the Zr-Sn alloy after polishing, AN treatment, immersing in SBF for 1 day and 4 days*

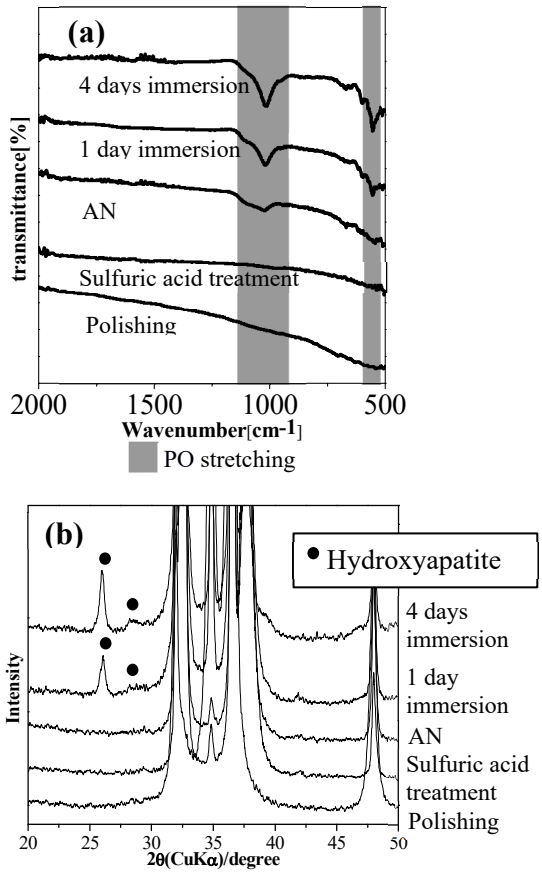

Fig. 6. (a) *FT-IR and* ***(b)*** *TF-XRD profiles of the surface of the untreated Zr-Sn alloy, the Zr-Sn alloy after polishing sulfuric acid treatment, AN treatment, immersing in SBF for 1 day and 4 days*

Fig. 6 shows the FT-IR profiles and the TF-XRD profiles of the surface of the Zr-Sn alloy after polishing, the Zr-Sn alloy with the sulfuric acid treatment, Zr-Sn alloy with micropores after AN treatment, the Zr-Sn alloy with both micropores and AN after immersing in SBF 1 day and 4 days. In the case of the Zr-Sn alloy with micropores, we obtained similar results as the case of Zr-Sn alloy without micropores. The FT-IR spectra shows the P-O stretching around 560 cm^{-1} and around 1000 cm^{-1} after the AN treatment, and the TF-XRD profile did not show the detection of diffraction peaks of calcium phosphate crystals such as hydroxyapatite. It is suggested that the AN formed on the surface of the Zr-Sn alloy with the sulfuric acid treatment were also amorphous-like calcium phosphate. From the Fig. 5 and Fig. 6, furthermore, the P-O stretching was detected in the both FT-IR profiles after immersion in SBF for 1 day and 4 days and the transmittance of the P-O stretching increased as the time increased. In addition, the diffraction peaks of hydroxyapatite were observed around 26 ° and 28 ° in the both TF-XRD profiles after immersion in SBF for 1 day and 4 days and the intensity of these diffraction peaks increased as the time went by. It is indicated that hydroxyapatite were induced by the function of AN for 1 day soaking in SBF, and also hydroxyapatite grew by soaking in SBF for 4 days. Diffraction peaks of hydroxyapatite around 32 ° were overlapped with those of the Zr-Sn alloy substrates.

Fig. 7 shows the SEM image and EDX profile of the surface of the Zr-Sn alloy without and with micropores with AN after immersion in SBF for 1 day. Fig. 8 shows those after immersion in SBF for 4 days. It was observed that the whole surface of the Zr-Sn alloy plates was covered with fake-like crystallites specific to bone-like apatite in both conditions regardless of the existence of micropores. From the EDX, the Ca peaks were strongly detected in comparison with those before soaking in SBF. It is indicated that the Zr-Sn alloy with AN treatment induced the formation of hydroxyapatite within 1 day in SBF and showed the high bioactivity. Comparing SEM image and EDX line-scanning of Zr-Sn alloy soaking in SBF for 1 day with 4 days, moreover, the size of flake-like crystals increased, and the intensity of Ca peaks expanded as the soaking time increased. This means that the hydroxyapatite crystals grew as the time increased.

The results of SEM, EDX and XRD indicated that the bone-like apatite covered with the whole surface of the Zr-Sn alloy within 1 day immersion in SBF by the AN treatment regardless of the sulfuric acid treatment. In addition, the growth of the apatite layer was shown as the immersion time increased. This means that the high

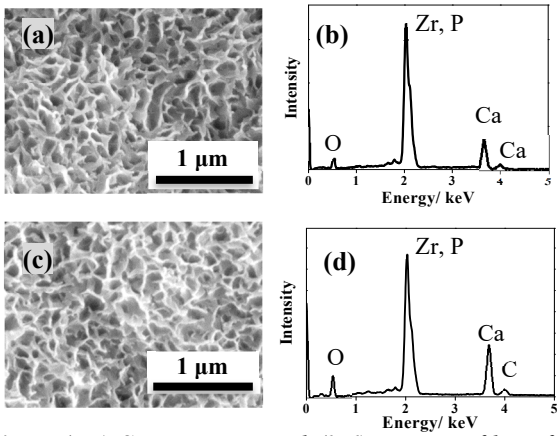

Fig. 7 (a,c) *SEM images and* ***(b,d)*** *EDX profiles of the surface of the Zr-Sn alloy* ***(a,b)*** *without micropores and* ***(c,d)*** *with micropores with AN after immersing in SBF for 1 day*

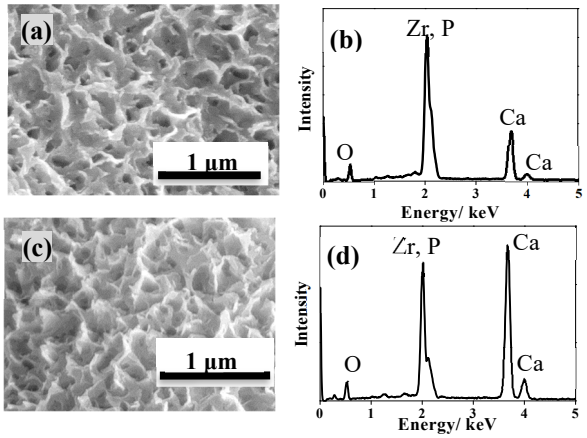

Fig. 8. (a,c) *SEM images and* ***(b,d)*** *EDX profiles of the surface of the Zr-Sn alloy* ***(a,b)*** *without micropores* ***(c,d)*** *with micropores and with AN after immersing in SBF for 4 days*

bioactivity was attained to the bioinert Zr-Sn alloy by AN treatment.

Fig. 9 shows the amount of Ca on the substrate (10×10×0.914 mm^3 in size) after the AN treatment and **(b)** after immersion in SBF for 1 day, 4 days and 14 days. The results before and after immersion in SBF showed the increase of Ca. The SEM images and ICP results before and after immersion in SBF showed that the AN changed to bone-like apatite by immersing in SBF and the consumption of Ca in SBF were occurred in the process of changing the shape of formed compound regardless of the existence of micropores. In addition, the ICP results showed the increase of Ca amount as the time increased in the case of Zr-Sn alloy both without and with micropores. Comparing Ca amount formed on the Zr-Sn alloy plate without and with micropores, Ca amount formed on the plate with micropores showed more amount than that formed on the plate without micropores. It is considered that the increase of surface roughness contributed to increase of the solution that contacted with the surface. The more solution contacted with the surface, the more AN was precipitated and thus the increase of Ca amount was shown after the AN treatment. Furthermore, the increase of the precipitated AN triggered further apatite formation and the improvement of Ca amount after soaking in SBF. These results mean that the apatite grew as the time increased and apatite-forming ability of the plate with micropores were superior to that of the plate without micropores.

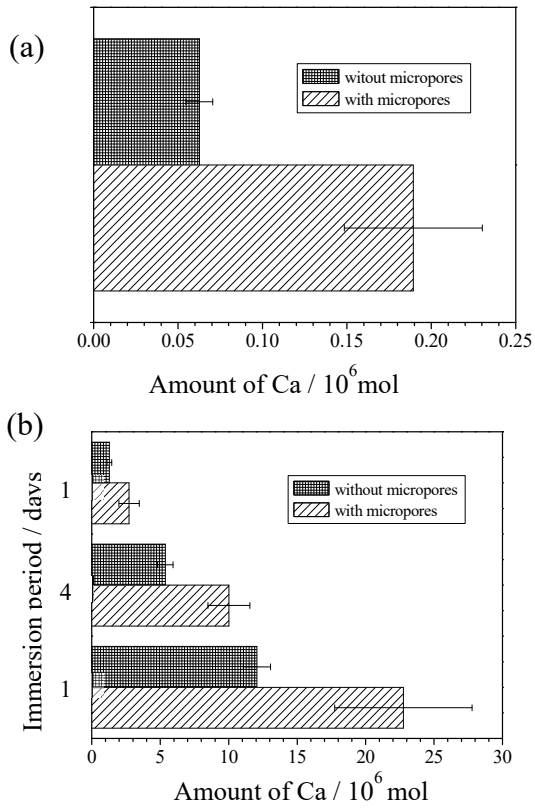

Fig. 9. *Amount of Ca on the substrate (10×10×1 mm^3 in size)* ***(a)*** *after the AN treatment and* ***(b)*** *after subsequent immersion in SBF for 1 day, 4 days and 14 days*

Fig. 10 shows the SEM images and the line scanning EDX profile of the cross-section of the Zr-Sn alloy with micropores after 14 days immersion in SBF. From the EDX line scanning, strong Ca peak were appeared at the point of 10 μm and the Ca peaks were kept strong in the section between the point of 10 μm and that of 27 μm. In addition, the Ca peak gradually decreased when the section arrived at the point of 27 μm which regarded as the boundary between the apatite layer and the Zr-Sn alloy. This means that hydroxyapatite was formed in the section between the point of 10 μm and that of 27 μm, and the coating thickness of hydroxyapatite layer formed on the surface of the Zr-Sn alloy were around 17 μm. In this measurement, the coating thickness of apatite layer of Zr-Sn alloy without micropores after 14 days immersion in SBF was not measured because of the thin coating thickness of apatite layer. From the result of ICP, however, the coating thickness was speculated as around 10 μm because the Ca amount is about half comparing with that of Zr-Sn alloy with micropores.

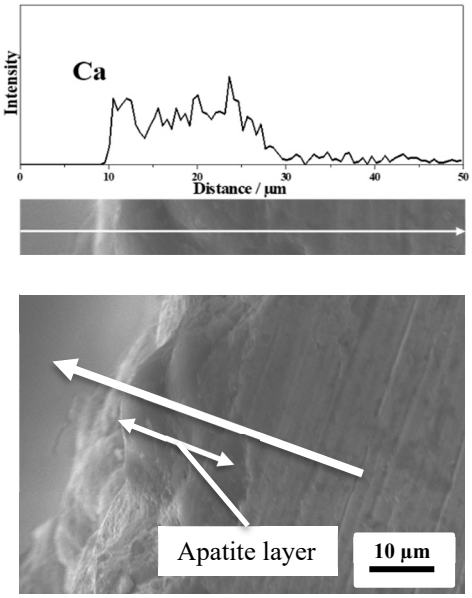

Fig. 10. *Cross-sectional SEM images and EDX line-scannning profile of the Zr-Sn alloy with AN after immersing in SBF for 14 days*

Apatite-forming ability was successfully attainted to bioinert Zr-Sn alloy within 1 day by the AN treatment regardless the conduction of the sulfuric acid treatment. However, the apatite-forming ability of bioactive Zr-Sn alloy with sulfuric acid treatment were superior to that of bioactive Zr-Sn alloy without sulfuric acid treatment. It is speculated that the difference of apatite-forming ability caused by the difference of surface roughness. As the surface roughness increased, the amount of AN precipitated on the surface of Zr-Sn alloy were considered to be increased. As the result, the amount of apatite induced by the AN were increased and the apatite-forming ability were improved.

The Zr-Sn alloy obtained apatite-forming ability within 1 day by this method, and this method is considered to be useful method because the period that pure Zr expressed bioactivity was reported more than 4 days [5]. In addition, it was reported that pure Ti showed apatite-forming ability within 1 day by NaOH and subsequent heat treatment [21] and this method has been applied to practical use as hip joint. Therefore, this method applying precipitation of the AN on the surface of the Zr-Sn alloy has the almost similar ability to impart apatite-forming ability as the practical use method, and this method will be expected to be applied to medical implant with bone-bonding ability. This result suggests that the precipitated AN induced apatite formation and enhanced apatite-forming ability.

Adhesive strength of the apatite film respect to the Zr-Sn alloy plate without micropores was 4.28 ± 1.40 MPa. Fig.11 shows the SEM image and the EDX profile of the substrate side fracture surface of the Zr-Sn alloy without micropores formation. The SEM image of fracture surface of the Zr-Sn alloy plate showed the observation of the Zr-Sn alloy plate on the almost fracture surface and also Ca peaks were clearly detected from the EDX scanning. Fig.12 shows the SEM image and the EDX profile of their fracture surface in jig side. The SEM image showed that the whole surface of jig covered with apatite, and the EDX scanning showed the stronger Ca peaks. From these results, it is indicated the fracture was occurred almost between the metal plate and formed apatite layer.

Adhesive strength of the apatite film respect to Zr-Sn alloy plate with micropores was 6.66 ± 2.86 MPa. Fig.13 shows the SEM image and the EDX profile of the substrate side fracture surface of the Zr-Sn alloy with micropores formation. The SEM image of fracture surface of the Zr-Sn alloy plate shows the almost all surface was covered with apatite. From the result of the EDX scanning, the strong peaks of Ca were detected. These results showed almost all fracture surface of Zr-Sn alloy plates were covered with hydroxyapatite. Fig.14 shows the SEM image and EDX profile of their fracture surface in jig side. The SEM image showed the whole fracture surface in jig side covered with apatite, too. Their EDX scanning showed the strong Ca peaks, too. These results show that the whole fracture surface of the Zr-Sn alloy plate were covered with hydroxyapatite. The results of the SEM and EDX of each fracture surface indicated that the fracture was occurred almost inside the apatite layer. This means the adhesive strength between the apatite layer and the Zr-Sn alloy plate were more than tensile strength of the formed hydroxyapatite. Therefore, adhesive strength of the apatite layer more than tensile strength of the formed apatite was attained to the Zr-Sn alloy by the combination of acid treatment and AN treatment. This is considered that in the case of Zr-Sn alloy with micropores, interlocking effect between the plate and apatite film was obtained because the apatite formation was induced in the micropores formed by the sulfuric acid treatment. Although the value of adhesive strength of bioactive Zr-Sn alloy was high, on the other hand, this value was lower than that of between Zr plate and apatite layer, Ti or Ti alloy plates and apatite layer as reported in our previous studies [14,16] and between the Ti or Ti alloys conducted the NaOH and subsequent heat treatment and apatite layer [23]. It suggested the stress concentration to apatite layer is the important factor of the value of adhesive strength, and the fracture in apatite layer was influenced by stress concentration caused by the shape of micropores. Therefore, it is expected to improve the adhesive strength value more by optimizing the micropores shape or adjusting the immersion days in sulfuric acid and the concentration of sulfuric acid and observing the cross-section.

We acknowledge several limitations in this report. First, changes in thickness of apatite layer was not evaluated. By taking into consideration the presented ICP experiments and this point, mechanism of apatite growth might be clarified. Second, effect of the acid treatment on chemical contribution of apatite formation and apatite adhesion on the surface of the plate was not investigated. In order to clarify this point, new other experiments are

needed such as X-ray photoelectron spectroscopy for all the condition of samples. Third, test of cell activity and bone formation on each plate have not been conducted yet. These points will be studied in our future study.

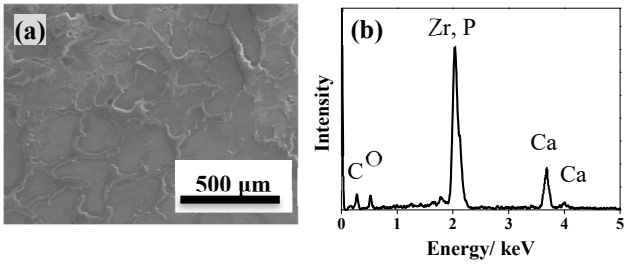

Fig. 11. (a) *SEM image and* ***(b)*** *EDX profile of the substrate side fracture surface of the Zr-Sn alloy without micropores and with AN after immersing in SBF for 14 days*

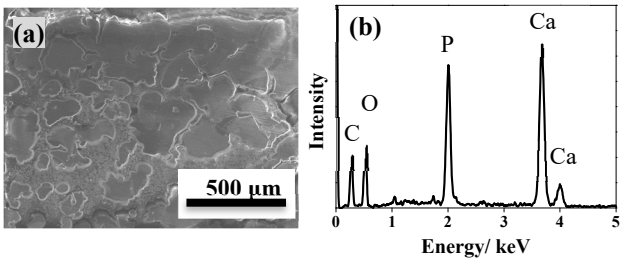

Fig. 12. (a) *SEM image and* ***(b)*** *EDX profile of the jig side fracture surface of the Zr-Sn alloy without micropores and with AN after immersing in SBF for 14 days*

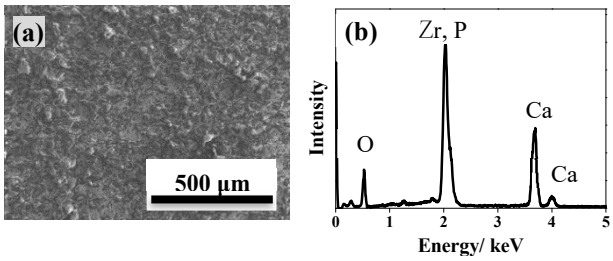

Fig. 13. (a) *SEM image and* ***(b)*** *EDX profile of the substrate side fracture surface of the Zr-Sn alloy with micropores and AN after immersing in SBF for 14 days*

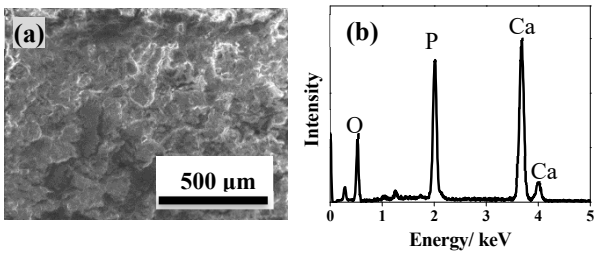

Fig. 14. (a) *SEM image and* ***(b)*** *EDX profile of the jig side fracture surface of the Zr-Sn alloy with micropores and AN after immersing in SBF for 14 days*

4. Conclusions

We succeeded in giving high bioactivity to bioinert Zr-Sn alloy and developing bioactive Zr-Sn alloy by forming micropores on their surfaces with sulfuric acid treatment and precipitating AN in the pores with AN treatment. By soaking in SBF, it was observed that hydroxyapatite covered the whole surface of Zr-Sn alloy with AN treatment within 1 day. Comparing Zr-Sn alloy without and with sulfuric acid treatment, in addition, apatite-forming ability of that with sulfuric acid treatment was superior to that without sulfuric acid treatment. The adhesive strength between apatite layer and Zr-Sn alloy plate showed more than tensile strength of the formed apatite. This material is promising to be useful for various biomaterial applications in the field of orthopedic surgery materials and density materials by their high bioactivity as well as excellent mechanical performance and low magnetic susceptibility.

5. Acknowledgments

This work was partly supported by The Foundation for the Promotion of Ion Engineering.

6. References

[1] Chellappa, M., Vijayalakshmi, U.: ‘In-situ fabrication of zirconium-titanium nano-composite and its coating on Ti-6Al-4V for biomedical applications’ IET Nanobiotechnol., 2017, 11, pp 83-90

[2] Zhou, F.Y., Qiu, D.J., Bian, D. et al.: ‘A Comparative in vitro Study on Biomedical Zr-2.5X (X = Nb, Sn) Alloys’, J. Mater. Sci. Technol., 2014, 30, pp 299-306

[3] Yan, Y., Han, Y.: ‘Structure and bioactivity of micro-arc oxidized zirconia films’, Surf. Coat. Technol., 2007, 201, pp 5692-5695.

[4] Akahori, T., Niinomi, M., Nakai, M., et al.: ‘Material Properties and Biocompatibilities of Zr-Nb System Alloys with Different Nb Contents for Biomedical Applications’, J. Japan Inst. Metals, 2011, 75, pp 445-451

[5] Uchida, M., Kim, H.-M., Miyaji, F., et al.: ‘Apatite formation on Zr metal treated with aqueous NaOH’, Biomaterials 2002, 23, pp 313-317

[6] Sandhyarani M., Rameshbabu N., Venkateswarlu K., et al.: ‘Fabrication, characterization and in-vitro evaluation of nanostructured zirconia/ hydroxyapatite composite on Zr’, Surf. Coati. Technol., 2014, 238, pp 58-67

[7] Aktuğ, S.L., Durdu, S., Yalçın, E., et al.: ‘Bioactivity and biocompatibility of hydroxyapatite-based bioceramic coatings on Zr by plasma electrolytic oxidation’, Mater. Sci. Eng. C, 2017, 71, pp 1020-1027

[8] Kokubo, T.: “Bioceramics and their clinical applications” (Woodhead Publishing, 2008)

[9] Kokubo, T., Kushitani, H., Sakka, S., et al.: ‘Solutions able to reproduce in vivo surface-structure changes in bioactive glass-ceramic A-W’, J. Biomed. Mater. Res., 1990, 24, pp 721-734

[10] Kokubo, T., Takadama, H.: 'How useful is SBF in predicting in vivo bone bioactivity?', Biomaterials, 2006, 27, pp 2907-2915

[11] Takadama, H., Kokubo, T.: 'In vitro evaluation of bone bioactivity', in T. Kokubo (Ed.): 'Bioceramics and their clinical applications' (Woodhead Publishing, 2008), pp 165-182

[12] Yao, T., Hibino, M., Yamaguchi, S., et al.: 'Method for stabilizing calcium phosphates fine particles, method for manufacturing calcium phosphates fine particles by using the method, and use thereof', U.S. Patent, 2012, 8178066, Japanese Patent, 2013, 5261712

[13] Yao, T., Hibino, M., Yabutsuka, T.: 'Method of producing bioactive complex material', U.S. Patent, 2013, 8512732, Japanese Patent, 2013, 5252399

[14] Yabutsuka, T., Karashima, R., Takai, S., et al.: 'Effect of Doubled Sandblasting Process and Basic Simulated Body Fluid Treatment on Fabrication of Bioactive Stainless Steels', Materials, 2018, 11, 1334

[15] Yabutsuka, T., Mizutani, H., Takai, S., et al.: 'Fabrication of Bioactive Co-Cr-Mo-W Alloy by Using Doubled Sandblasting Process and Apatite Nuclei Treatment', Trans. Mat. Res. Soc. Japan, 2018, 43, pp 143-147

[16] Yabutsuka, T., Mizuno, H., Takai, S.: 'Fabrication of bioactive titanium and its alloys by combination of doubled sandblasting process and alkaline simulated body fluid treatment', J. Ceram. Soc. Japan, 2019, 127, pp 669-677

[17] Kidokoro, T., Yabutsuka, T., Takai, S., et al.: 'Bioactivity Treatments for Zr and Ti-6Al-4V Alloy by the Function of Apatite Nuclei', Key Eng. Mater., 2016, 720, pp 175-179

[18] ISO 23317: 'Implants for Surgery—In vitro evaluation for apatite-forming ability of implant materials', 2014

[19] Lacefield, W.R.: 'Hydroxyapatite Coatings', in Hench, L.L. (Ed.): 'An Introduction to Bioceramics' (Imperial College Press, 2013, 2nd edn.), pp 331-347

[20] Kim, H.-M., Miyaji, F., Kokubo, T., et al.: 'Bonding strength of bonelike apatite layer to Ti metal substrate', J. Biomed. Mater. Res., 1997, 38, (2), pp 121-127

[21] Yamaguchi, S., Takadama, H., Matsushita, T., et al.: 'Cross-sectional analysis of the surface ceramic layer developed on Ti metal by NaOH-heat treatment and soaking in SBF', J. Ceram. Soc. Japan, 2009, 117, pp 1126-1130

[22] Kim, H.-M., Miyaji, F., Kokubo, T., et al.: 'Preparation of Bioactive Ti and Its Alloys via Simple Chemical Surface Treatment', J. Biomed. Mater. Res., 1996, 32, pp 409-417

[23] Ban, S., Iwaya, Y., Kono, H., et al.: 'Surface modification of titanium by etching in concentrated sulfuric acid', Dent. Mater., 2006, 22, (12), pp 1115-1122